scientific reports

Check for updates

OPEN

ZIP13 marks muscle satellite cells and contributes to their quiescent and active phase balance

Emi Yoshigai[1,2,4]✉, Takafumi Hara[1,4], Masaki Hashimoto[1], Hidenao Tsuzuki[1], Takaya Abe[3], Kenichi Inoue[3], Ayaka Noguchi[1], Takuto Ohashi[1] & Toshiyuki Fukada[1]✉

Loss of ZIP13 causes Ehlers-Danlos syndrome spondylodysplastic type 3 involving connective tissue dysplasias associated with a reduction in muscular strength. However, ZIP13 role in skeletal muscle homeostasis, particularly for the regulation of muscle satellite cells (MuSCs), remains poorly understood. In this study, we investigated *Zip13*-knockout (KO) mice and found a reduction in MuSCs of *Zip13*-KO mice, in which the quiescent and activated phase balances were disrupted. To clarify the physiological role and dynamics of ZIP13 expression in MuSCs, we generated *Zip13-GFP* knock-in (KI) mice encoding *GFP* at the *Zip13* locus, which showed that ZIP13 contributes to the phase balance regulation of quiescent and activated MuSCs and their functions. Indeed, *Zip13*-KO mice exhibited delayed recovery from skeletal muscle injury, indicating ZIP13 requirement for proper skeletal muscle regeneration. Moreover, GFP expression was reduced in the MuSCs of homozygous *Zip13-GFP* KI mice whose intact ZIP13 expression was perturbed, suggesting that positive feedback mechanisms exist to maintain ZIP13 expression. Altogether, our results illustrate that ZIP13 might be positively involved in skeletal muscle regeneration by controlling the quiescent/activated phase balance of MuSCs through autoregulatory ZIP13 expression, and that newly generated *Zip13-GFP* KI mice would be useful for investigating the roles and dynamics of ZIP13-expressing cells.

Keywords ZIP13, Muscle satellite cells, Skeletal muscle regeneration

Skeletal muscle, which contains approximately 60% of the body's total zinc, is essential for motor function[1]. Maintaining skeletal muscle function is crucial not only for preserving physical capabilities and sustaining quality of life but also for preventing age-related decline, including sarcopenia and frailty[2]. Recent studies have linked decreased intracellular zinc levels to aging and age-related diseases. However, the role of zinc in the generation, regeneration, and function of skeletal muscles remains unclear, especially in skeletal muscle-related diseases such as sarcopenia and locomotive syndrome. Currently, there is a lack of effective therapeutic treatments for these diseases, highlighting the urgent need to elucidate the pathophysiological mechanisms underlying the development of new therapeutic strategies.

Zinc, an essential trace element, plays an indispensable role in the maintenance of protein structure and function, including those of enzymes, transcription factors, and signaling molecules. The significance of zinc as an essential mineral was established in 1961 by Prasad et al.[3–5], who demonstrated that zinc deficiency disrupts cellular homeostasis and causes growth impairment, particularly in skeletal muscles[4]. Zinc deficiency precipitates various metabolic disorders, whereas excess zinc can induce cytotoxicity, so that its homeostasis should be tightly regulated in cells. Mammalian cells have evolved two transporter families, Zrt/Irt-like protein (ZIP, SLC39A) and ZnT (SLC30A), that stringently regulate zinc homeostasis. ZIP transporters facilitate the influx of zinc ions into the cytoplasm, whereas ZnT transporters mediate the efflux of zinc from the cytoplasm into the extracellular space and intracellular organelles, thereby modulating cellular zinc localization, which is crucial for diverse cellular responses[6]. Recent research has implicated zinc transporters in numerous signaling pathways and their dysfunction is associated with several human diseases, suggesting that targeting zinc transporters could provide novel therapeutic potential[6].

SLC39A13/ZIP13 is a member of the ZIP transporter family[6] which has been implicated in human diseases with various connective tissues dysplasia. Our and other research groups have identified that pathophysiological

[1]Molecular and Cellular Physiology, Faculty of Pharmaceutical Sciences, Tokushima Bunri University, 180 Nishihama-Boji, Yamashiro, Tokushima 770-8514, Japan. [2]JSPS Research Fellowship for Young Scientists, Tokyo, Japan. [3]Laboratory for Animal Resources and Genetic Engineering, RIKEN Center for Biosystems Dynamics Research, 2-2-3 Minatojima-minamimachi, Chuo-ku, Kobe, Hyogo 6500047, Japan. [4]These authors contributed equally: Emi Yoshigai and Takafumi Hara. ✉email: emi-yoshigai@ph.bunri-u.ac.jp; fukada@ph.bunri-u.ac.jp

mutations in the SLC39A13/ZIP13 gene are responsible for Ehlers-Danlos Syndrome Spondylodysplastic Type 3 (EDSSPD3, OMIM 612350), an autosomal recessive connective tissue disorder suffering short stature, skeletal malformations, spinal deformities, fragile skin, and hypodontia[7–10], which has been documented in approximately ten patients to date in the world[7–9,11,12]. Our recent study demonstrated an increase in *Zip13* gene expression during myogenesis and revealed that knockdown of ZIP13 in C2C12 mouse myoblasts impedes myogenic differentiation[13]. We also utilized induced pluripotent stem cells (iPSCs) derived from EDSSPD3 patients to elucidate the pathophysiological mechanisms underlying ZIP13 dysfunction in muscle formation. We confirmed that myocytes differentiated from EDSSPD3-iPSCs exhibited impaired myogenic differentiation, which was restored upon correction of pathological mutations in ZIP13 by gene editing. These findings indicate that ZIP13 is a potential myogenic regulatory factor that is crucial for skeletal muscle formation[13]. Nevertheless, it remains unclear the role of ZIP13 in muscle satellite cells (MuSCs) which is crucial for the early development, differentiation, and recovery of skeletal muscles from injury.

MuSCs possess stem cell properties that are central to muscle regeneration and repair through the maintenance of quiescent and activated states. Quiescent satellite cells reside on the surface of muscle fibers[14]. Upon stimulation with extracellular factors initiating early muscular development, or physical stimuli such as muscle injury, MuSCs transition to an activated state, proliferating, and differentiating to form new muscle fibers, which is an essential step for development and repair[15] where MRFs, including Pax7[16–21], MyoD[22–25], and Myf5[26,27] are crucially involved. Additionally, muscle atrophy such as sarcopenia disrupts the regulatory mechanisms responsible for maintaining the stem cell pool, which depend on the transition between quiescent and activated states[28]. Therefore, the proper phase control of MuSCs between quiescence and activation relies on precise regulatory mechanisms that are important for accurate muscular homeostasis.

The quiescence phase MuSCs expressing integrin α7 (ITGA7) and CD34 maintain dormancy until activated by signals from the surrounding environment[29]. Damage or stress also triggers activation of MuSCs through the signaling pathways involving growth factors, cytokines, and hormones, providing the necessary environment for muscle regeneration[28,30–32]. During activation, satellite cells further differentiate, contributing to the formation of new muscle fibers that express Myf5, MyoD[33], and Myogenin[24] to promote differentiation into muscle cells. Experimental myocyte differentiation from the iPS cells and C2C12 cells in our previous study[13] would not take place via MuSCs, therefore, the involvement of ZIP13 in MuSC functions and their homeostasis, has not been demonstrated so far.

In this study, we focused on the role of ZIP13 in MuSCs which are pivotal for skeletal muscle formation and regeneration, by analyzing the mechanisms involving ZIP13 using our developed *Zip13-GFP* knock-in (KI) mice and *Zip13* knockout (KO) mice. We observed a reduction in the number of MuSCs in *Zip13*-KO mice, in which the quiescent/activated phase balance of MuSCs was disrupted. Analysis MuSCs of *Zip13-GFP* KI mice revealed that the GFP expression level was higher in the quiescent-phase MuSCs than in the activated phase, indicating that ZIP13 may contribute to the regulation of the quiescent/activated phase balance of MuSCs. We also found that delayed muscle injury recovery occurred due to the loss of ZIP13, illustrating that ZIP13 expression in MuSCs is required for the proper regeneration of skeletal muscle. These results suggest that ZIP13 may be involved in skeletal muscle regeneration by contributing to the quiescent and activated phase balance of MuSCs.

Results

Zip13 deletion effects on the properties of MuSCs

Given the muscle hypotonia observed in EDSSPD3 patients who have a genetic loss-of-function mutation of ZIP13[13], and the fact that patient-derived iPS cells showed impaired myogenic differentiation, we assumed the intrinsic role of ZIP13 in the early development of skeletal muscle. Therefore, we evaluated the expression of MRFs in the skeletal muscles of *Zip13*-KO mice, showing a decreasing tendency of gene expression of MRFs, such as *Pax7, Pax3, MyoD,* and *Myf5*, in the gastrocnemius muscles of *Zip13*-KO mice (Fig. 1A). This suggests that ZIP13 deficiency perturbs the precise regulation of skeletal muscle homeostasis, implicating ZIP13 in muscular homeostasis. To investigate the involvement of ZIP13 in the early stages of skeletal muscle differentiation, we assessed the *Zip13*-KO mice driven MuSCs (*Zip13*-KO MuSCs) and found that ITGA7-positive MuSCs were reduced in *Zip13*-KO mice compared with WT mice (Fig. 1B, C and Supplemental Fig. 1). Gene expression analysis revealed that *Ki67* expression was higher in *Zip13*-KO MuSCs than in WT MuSCs (Fig. 1D), suggesting that ZIP13 affects MuSC phase determination. We then assessed the ratio between the quiescent (ITGA7-positive and CD34-positive) and activated (ITGA7-positive and CD34-negative) states of *Zip13*-KO MuSCs and found a significant decrease in quiescence and an increase in activated states in *Zip13*-KO MuSCs (Fig. 1E). These results indicated that ZIP13 may play a role in maintaining MuSCs in a quiescent state; therefore, its deficiency disrupts the homeostatic balance of the quiescent and activated states of MuSCs.

Visualization of the ZIP13-expressing MuSCs

Given the role of ZIP13 in regulating the balance between the quiescent and activated states of MuSCs, we investigated whether changes in ZIP13 expression in MuSCs occurred in a state-dependent manner. To visualize ZIP13 expression levels using the GFP signal, we generated *Zip13-GFP*-KI mice by inserting an EGFP-IRES-CreERT2 cassette into exon 2 of the *Zip13* locus (Fig. 2A). As shown in Fig. 2B, a GFP-positive population was confirmed in ITGA7-positive MuSCs from *Zip13-GFP*-KI mice using FACS analysis. We then assessed MuSCs marked with PAX7, another MuSC marker, and found that the isolated PAX7-positive MuSCs expressed GFP (Fig. 2C), suggesting that the *Zip13* promoter was activated in MuSCs; therefore, they theoretically expressed *Zip13* mRNA. Furthermore, GFP signals were upregulated during the quiescent phase of MuSCs (Fig. 2D, left), which was also true for the gene expressions of *Zip13* and *GFP* (Fig. 2D, right). These results suggest that ZIP13 expression is upregulated in the quiescent state of MuSCs and that ZIP13 may functionally orchestrate the balance between the quiescent and activated states of MuSCs.

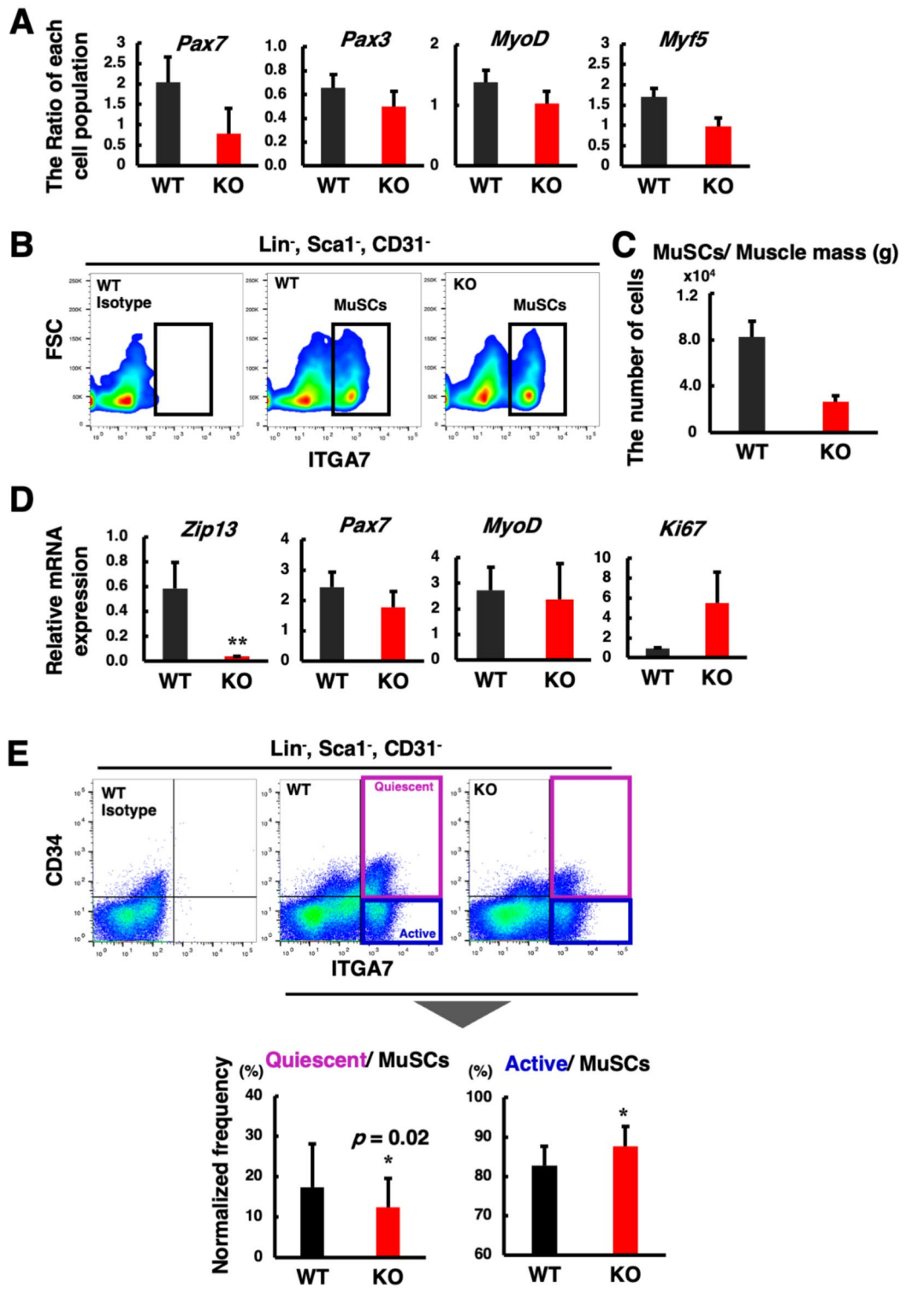

Fig. 1. Properties of MuSCs in *Zip13*-KO mice. (**A**) mRNA expressions of MRFs in the skeletal muscle of *Zip13*-KO mice. (**B**) Cell populations of ITGA7 positive MuSCs. The cells derived from hind legs of either WT or *Zip13*-KO mice were analyzed using FACS. The ITGA7 positive MuSCs were gated based on the fluorescent intensity derived from the fluorescent-labeled isotype control antibody. (**C**) The number of ITGA7-positive MuSCs of WT and *Zip13*-KO mice were normalized using either muscle mass or the number of viable cells. (**D**) mRNA expressions of *Zip13* and MuRFs in ITGA7-positive MuSCs as shown in (**B**). (**E**) The FACS analysis of the active and quiescent MuSCs of either WT or *Zip13*-KO mice. The ITGA7 and CD34 positive populations were gated based on the fluorescent intensity derived from the fluorescent-labeled isotype control for either ITGA7 or CD34 antibodies. A ration of the quiescent- and active-phase MuSCs gated as purple and blue squares (dot plots), respectively, were quantified (bar graphs). Student's *t*-test was used to compare the two groups. Values are means ± S.E. of 6 mice. The asterisk indicates a significant difference (*$p < 0.05$).

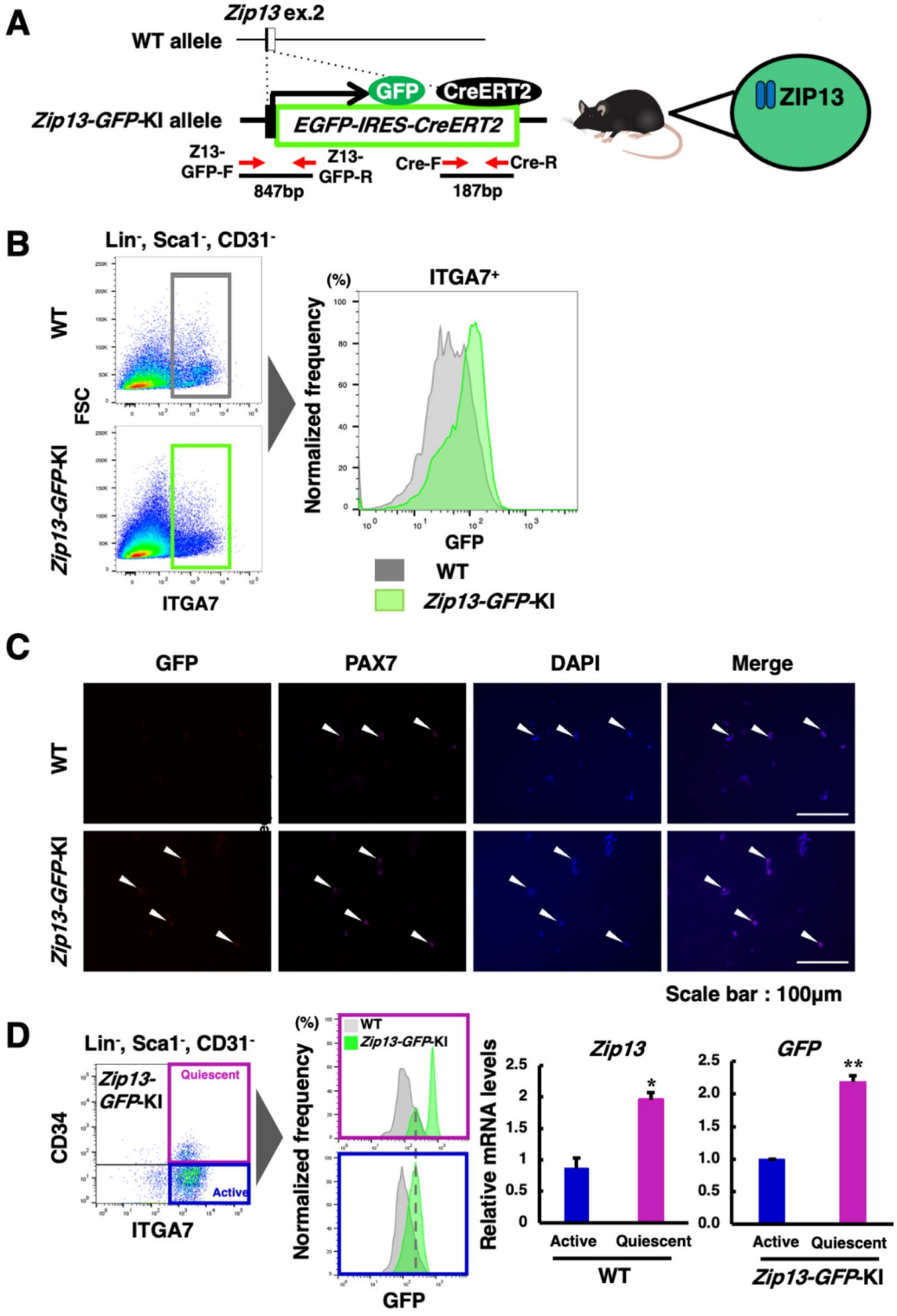

To further analyze the transition between quiescent and activated states of ZIP13-expressing MuSCs, we crossed *Zip13-GFP*-KI mice with Rosa26-tdTomato reporter mice to generate *Zip13-GFP/Tomato*-KI mice (Fig. 3A). Upon tamoxifen administration, CreERT2 is activated, which leads to the excision of the stop codon flanked by loxP sites at the Rosa26 locus of the reporter mouse, resulting in the expression of the downstream *Tomato* gene[34] (Fig. 3A and Supplemental Fig. 2). This enabled tracing of the cell lineage of ZIP13-expressing cells, even after the *Zip13* promoter became inactive. After tamoxifen injection, we co-stained *Zip13-GFP/Tomato*-KI mice-derived MuSCs with ITGA7, an MuSC marker. ITGA7-positive MuSCs expressed both GFP and Tomato proteins (Fig. 3B). Next, we assessed MuSCs marked with PAX7 and found that PAX7-positive cells were either Tomato alone (Fig. 3C, filled arrowhead, and Supplemental Fig. 3) or both GFP and Tomato (Fig. 3C, open arrowhead, and Supplemental Fig. 3), indicating that ZIP13 expression may change with MuSC status. Interestingly, Tomato-positive MuSCs showed slightly increased expression of *MyoD* which tend to be

◀**Fig. 2**. Visualization of ZIP13-expressing MuSCs in *Zip13-GFP*-KI mice. (**A**) A schematic diagram of the gene map of *Zip13-GFP*-KI mice. GFP-IRES-CreERT2 cassette was inserted into exon 2 (ex.2) of the *Zip13* gene locus. GFP and CreERT2 proteins are expressed in the cells expressing ZIP13. The positions of the genotyping primers were depicted as red arrows and the primer sequences were written in Methods. (**B**) FACS analysis of MuSCs of *Zip13-GFP*-KI mice. Representative dot plots and gating scheme to isolate mononucleated muscle satellite cells was shown. $CD45^-$, $CD31^-$, $CD11b^-$, and $Sca1^-$ cells were gated (left) and analyzed in ITGA7 expression (middle). The GFP expression in ITGA7 positive MuSCs was shown as histogram data (right). (**C**) Confirmation of the GFP expression of isolated MuSCs. The upper panel images were from WT mouse-isolated MuSCs. The lower panel images were from *Zip13-GFP*-KI mouse-isolated MuSCs. GFP and PAX7 were stained with the specific anti-GFP and anti-PAX7 antibodies, respectively. Nuclei were stained with DAPI. The scale bar represents 50 μm. (**D**) The FACS analysis of the active and quiescent MuSCs of either WT or *Zip13-GFP*-KI mice. The GFP fluorescent intensities of the quiescent and activated phase MuSCs gated as purple and blue squares (left dot plots), respectively, were analyzed as histogram data. Each phase of MuSCs was sorted and *Zip13* and *GFP* mRNA expressions were quantified using qPCR. Student's *t*-test was used to compare the two groups. Values are means ± S.E. of 3–4 mice. The asterisk indicates a significant difference ($*p < 0.05$, $**p < 0.01$).

expressed in an activated state[28,30,33] (Fig. 3D). Because Tomato-positive cells theoretically include progeny populations derived from GFP-positive cells that express ZIP13, these results suggest that ZIP13 may play a role in maintaining MuSCs in the quiescent phase.

ZIP13 is required for recovery from muscle injury

Next, we investigated whether ZIP13 was involved in muscular regeneration by applying an acute muscle injury model using $BaCl_2$ injection[35]. $BaCl_2$ was injected into the tibialis anterior (TA)/ gastrocnemius (GAS) muscles of WT and *Zip13*-KO mice, and the muscles were subjected to H&E staining for morphological evaluation[36].

Before injection, there was little obvious morphological difference between the WT and *Zip13*-KO mice (day 0: Fig. 4A, a and d). On Day 5 after $BaCl_2$ injection, WT mice suffered significant muscle damage with the accumulation of mononuclear cells, most likely due to acute inflammation, where the muscle nuclei were localized at the center of muscle fibers (day 5: Fig. 4A, b and e), which is commonly observed in the muscle when acute inflammation occurs[16,35], and then partly migrated to the peripheral region of muscle fibers during muscle regeneration (day 10: Fig. 4A, c, and Supplemental Fig. 4). In *Zip13*-KO mice, mononuclear cells remained on day 10, and migration of muscle nuclei to the periphery was also not completed (day 10: Fig. 4A, f, and Supplemental Fig. 4), indicating that muscle regeneration was delayed in *Zip13*-KO mice. Further, the area and the surrounding length of muscle fiber sections were analyzed at Day 0 and 10 post-injury to evaluate the delayed muscle regeneration in *Zip13*-KO mice. The muscle fibers with centrally placed nuclei were subjected to quantitative analysis on day 10. The area and length were slightly reduced on Day 10 compared to Day 0 in both WT and *Zip13*-KO mice. In addition, to evaluate the effect of lack of the *Zip13* expression in the muscle regeneration, Cohen's d values between day 0 and 10 in WT and *Zip13*-KO mice were calculated and showed that the values for perimeter and sectional area in *Zip13*-KO mice (1.06 and 0.88, respectively) were higher than those in WT mice (0.10 and 0.28), indicating the lack of *Zip13* gene is involved in the delayed muscle regeneration. Such observations may be reflected in gene expression patterns (Fig. 4B); expression levels of *Pax7*, *MyoD*, *Atrogin*, and *MuRF* were significantly reduced, indicating that prominent inflammation and delayed recovery of muscle regeneration occurred in *Zip13*-KO mice[37].

To determine whether the dynamics of ZIP13-expressing MuSCs occur during muscular regeneration, we applied $BaCl_2$ injection model with *Zip13-GFP/Tomato*-KI mice. We found that GFP signals were transiently reduced in quiescent MuSCs 20 days after $BaCl_2$ injection (light blue line in Fig. 4C, left panel) and then recovered 30 days after the injection (red line in Fig. 4C, left panels). In contrast, Tomato-positive cells in activated MuSCs were not reduced 20 days after $BaCl_2$ injection (light blue line in Fig. 4c, right panel). These results indicated that ZIP13 (GFP)-expressing quiescent MuSCs were converted to Tomato-expressing activated MuSCs, promoting the recovery of muscle injury and early muscle development and recovery processes.

Regulatory mechanisms of ZIP13 expression

To further analysis of the regulatory mechanisms of ZIP13 expression in MuSCs, we analyzed *Zip13-GFP*-KI homozygous mice whose open reading frame of *Zip13* was abrogated, rendering them theoretically identical to *Zip13*-KO mice. The GFP signals in MuSCs isolated from the homozygous mice were significantly reduced in both quiescent and activated MuSCs (red area of histograms in Fig. 5A) as compared in MuSCs from the heterozygous mice (green area of histograms), a reduction that was also observed during muscle regeneration process 40 days after $BaCl_2$ injection in the homozygous mice (red area of histograms in Fig. 5B). These results suggested that ZIP13 expression itself was required for the *Zip13* promoter activity in MuSCs.

Discussion

Skeletal muscle holds 60% of the total zinc in the body and plays an important role in motor functions[6]. Skeletal muscle health is closely related to healthy life expectancy, and recent studies have increasingly elucidated the relationship between age-related zinc reduction and associated diseases such as frailty[2]. However, the role of zinc in the skeletal muscle remains unclear. The zinc transporter family cooperatively regulates zinc homeostasis, strictly controlling the dynamics of zinc inside and outside the cells[6]. Recent studies have reported various diseases caused by genetic mutations in zinc transporters[6], highlighting the association between zinc transporters and disease mechanisms and their potential as drug targets[6]. We previously demonstrated that

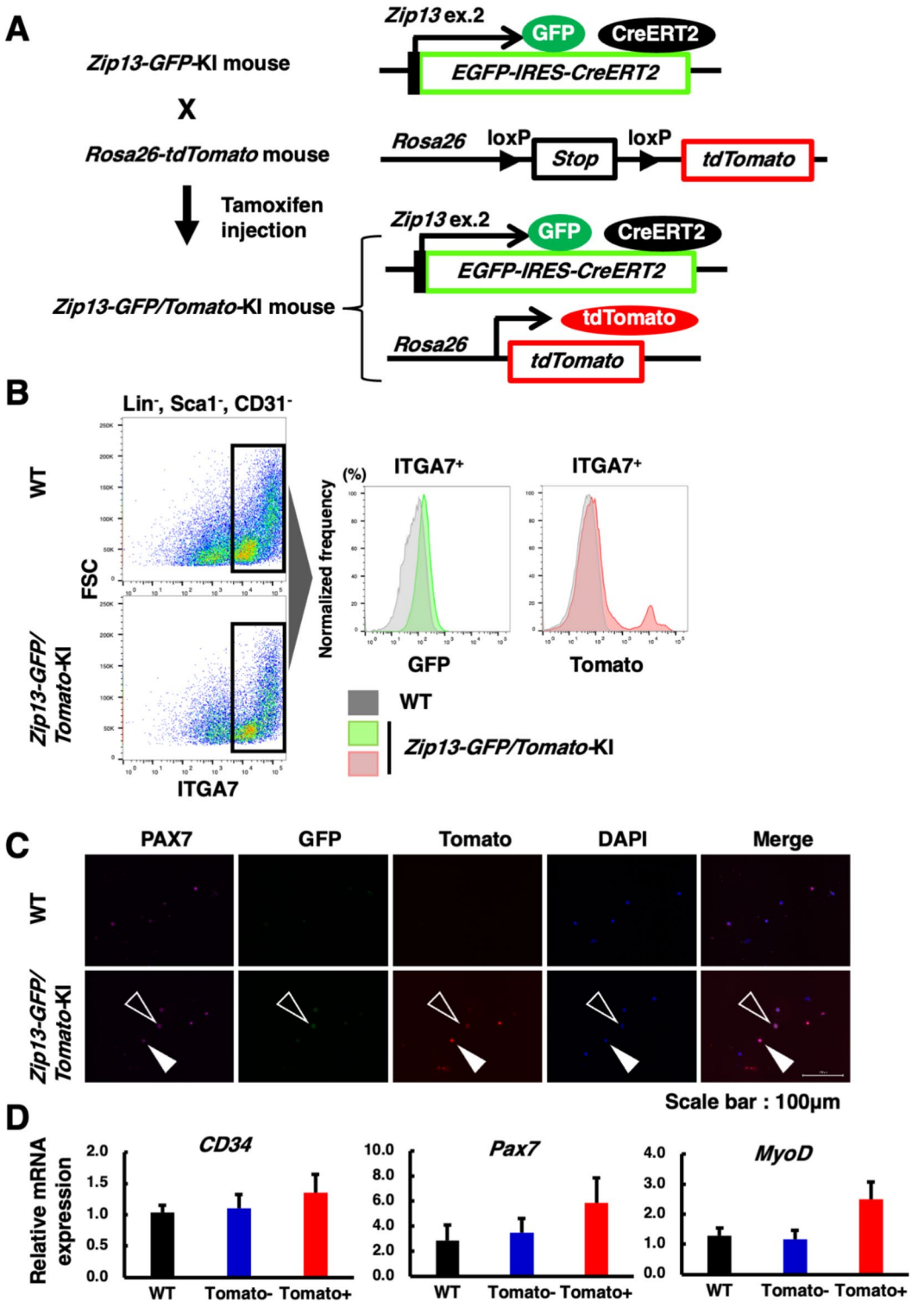

patients with EDSSPD3 caused by loss of function of ZIP13 muscular hypotonia (decreased muscle strength)[7]. Recent studies using iPS cells derived from EDSSPD3 patients have shown that ZIP13 is involved in muscle development and homeostasis[13]. Furthermore, ZIP13 plays a role in maintaining cardiovascular homeostasis[38]. However, the role of ZIP13 in skeletal muscle homeostasis, especially during the early stages of myogenesis, remains largely unexplored. Therefore, uncovering its molecular mechanisms could provide new insights into the regulation of muscle differentiation and regeneration.

MuSCs play a crucial role in early muscle development and regeneration, and regulate skeletal muscle differentiation[39–41]. Thus, intensive research has been conducted to elucidate the molecular mechanisms controlling the phase transition of MuSCs to develop therapeutic treatments for muscle-related disorders. Our previous studies revealed that ZIP13 plays a critical role in muscular function and myogenesis[7,13,42], although there have been no reports on the association between ZIP13 and MuSCs. We demonstrated that ITGA7-

◀**Fig. 3**. Visualization of the lineage of ZIP13-expressing MuSCs using *Zip13-GFP/Tomato*-KI mice. (**A**) A schematic diagram of the gene map of *Zip13-GFP/Tomato*-KI mice. *Zip13-GFP/Tomato*-KI mice were crossed with Rosa26-tdTomato mouse that is harboring the stop codon between loxP sites followed by tdTomato sequence on Rosa26 locus The pups were designated as *Zip13-GFP/Tomato*-KI mice. The tamoxifen injection in *Zip13-GFP/Tomato*-KI mice activated CreERT2 in the cells with the activated promoter for *Zip13* gene, and then activated CerERT2 induced the removal of the stop codon that promoted Tomato expression. (**B**) FACS analysis of MuSCs in *Zip13-GFP/Tomato*-KI mice. Representative FACS dot plots and gating strategy to purify mononucleated satellite cells were shown. $CD45^-$, $CD31^-$, $CD11b^-$, and $Sca1^-$ cells were gated and analyzed in ITGA7 expression. GFP and Tomato expression in ITGA7 positive MuSCs were analyzed as histogram data. (**C**) Confirmation of the GFP and Tomato expressions in isolated MuSCs. Pax7, GFP, and Tomato expression in MuSCs were examined in both WT- and *Zip13-GFP/Tomato*-KI mice. Pax7-positive MuSCs co-expressed with either Tomato (filled arrowhead) or GFP/Tomato (open arrowhead) were detected. Nuclei were stained with DAPI. The scale bar represents 100 μm. (**D**) Each Tomato positive and negative MuSCs as shown in the ((**B**), right histogram) was sorted and then *CD34*, *Pax7*, and *MyoD* mRNA expressions were quantified using qPCR. Values are means ± S.E. of 6 mice.

positive MuSCs were significantly reduced in *Zip13*-KO mice (Fig. 1C), suggesting that ZIP13 was required for their maintenance. In addition, ITGA7-positive MuSCs derived from *Zip13*-KO mice showed increased *Ki67* expression, indicating that the loss of ZIP13 increased the proliferative capacity of MuSCs (Fig. 1D), and quiescent phase MuSCs were significantly reduced in *Zip13*-KO mice (Fig. 1E). Given that various stimuli initiate the proliferative activity of MuSCs in the activated phase, leading to the progress of muscle differentiation[15,33], these results suggest that ZIP13 might play a role as a MRF-like factors that controls the fate decision of MuSCs in the transition between the quiescent and active phases.

Possible involvement of ZIP13 in the control of quiescent and active phase balance attempted us to clarify the expression and distribution of ZIP13 in MuSCs, therefore, we generated *Zip13-GFP*-KI mice that allowed us to investigate the expression profile of ZIP13 in MuSCs. We found that the GFP signal was expressed in both PAX7-positive and ITGA7-positive MuSCs (Fig. 2. B and C), in which the quiescent MuSCs expressed much higher levels of GFP and ZIP13 than the activated MuSCs (Fig. 2D). As quiescent phase MuSCs were reduced in *Zip13*-KO mice (Fig. 1E), these results suggested that ZIP13 plays a role in maintaining MuSCs in the quiescent phase. Namely, we demonstrated that (i) the loss of ZIP13 leads to a decrease in the number of quiescent MuSCs, (ii) ZIP13 expression primarily marked quiescent MuSCs, and (iii) ZIP13 expression levels changed according to the phase transition of MuSCs, all of which highlight that ZIP13 has the potential to be a valuable molecular marker for assessing quiescent satellite cells.

Among the molecules expressed in MuSCs, Pax7 and CD34 mark the quiescent phase of MuSCs and are critically involved in homeostasis. *Pax7*-KO mice exhibited a reduced number of MuSCs and delayed muscle regeneration[19]. Similarly, the absence of CD34 reduced the proliferation and motility of MuSCs[43]. Recognizing the critical role of ZIP13 in the poorly understood early steps of MuSC activation, it is essential to focus on the ZIP13-mediated regulatory mechanism of the phase transition of MuSCs to elucidate whether and how ZIP13 cooperates with other MuSC markers such as Pax7 and CD34 to regulate the transition from the quiescent to the activated phase. These results prompted us to further analyze the lineage of ZIP13-expressing MuSCs using newly generated *Zip13-GFP/Tomato*-KI mice, which are capable of tracing ZIP13-expressing MuSCs that express GFP and their progeny cells that express tomato (Fig. 3A). Tomato-positive MuSCs exhibited increased *MyoD* expression (Fig. 3D). Given that MyoD is more highly expressed in the activated phase of MuSCs than in the quiescent phase[22], Tomato-positive MuSCs may have activated MuSC properties. Since Tomato-positive MuSCs theoretically contain GFP-negative MuSCs that are used to express ZIP13, these results are another example showing that ZIP13 expression is associated with the balance of the quiescent and activated phases of MuSCs and that ZIP13 may control the transition from the quiescent to the activated state (Fig. 6).

If ZIP13 plays an important role in MuSCs, the question arises of what happens to muscle regeneration if ZIP13 function was lost. To address this point, we applied an acute muscle injury model using $BaCl_2$ intramuscular injection[35] to *Zip13*-KO mice and demonstrated that mononuclear cells were still heavily accumulated at the inflammation site, and the nuclei remained infiltrated at the center of the muscle fibers even on day 10 (Fig. 4A, f). The quantitative analysis of perimeter and cross sectional area of muscle fibers, with Cohen's d value between Day 0 and Day 10 for both WT and *Zip13*-KO mice, revealed significant differences in *Zip13*-KO compared to WT mice, suggesting that muscle recovery was delayed in KO mice, which was also indicated by expression changes in MRF genes (Fig. 4B), most likely due to the reduction of quiescent MuSCs in *Zip13*-KO mice (Fig. 2D). Since MuSC proliferation is slower than that of myoblasts[30,44,45], it is reasonable to consider that the reduction in quiescent MuSCs in *Zip13*-KO mice affected proper muscle regeneration. Given that ZIP13 marks quiescent MuSCs rather than activated MuSCs, we assessed whether ZIP13 expression changed the phase of MuSCs during muscle regeneration in an acute muscle injury model using *Zip13-GFP/Tomato*-KI mice. The number of GFP-expressing quiescent MuSCs decreased following muscle injury (Fig. 4C, left, light blue line). Intriguingly, Tomato-expressing activated MuSCs were maintained during muscle repair processes (Fig. 4C, right, red line), suggesting that the ZIP13 expressing quiescent MuSCs transitioned into Tomato-expressing activated MuSCs to fix the injured muscles.

One of intriguing findings was that a significant reduction in GFP signals in MuSCs isolated from *Zip13-GFP*-KI homozygous mice (Fig. 5A), which was theoretically identical to *Zip13*-KO mice. Reduction of GFP signals in MuSCs was also observed during muscle regeneration (Fig. 5B). Since GFP expression is dependent on *Zip13* promoter activity, these data suggest that ZIP13 expression itself is indispensable for the activation

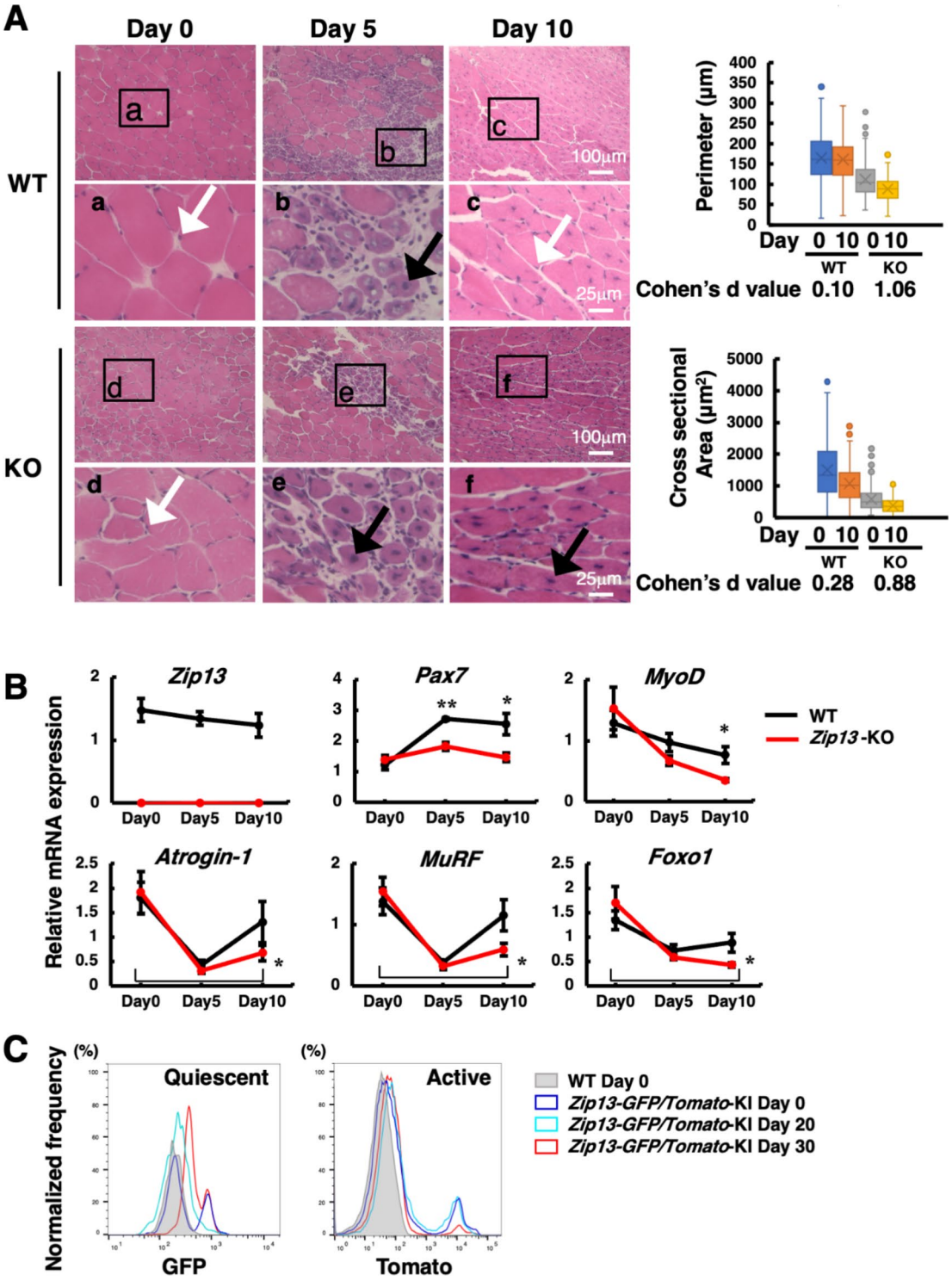

of *Zip13* promoter, which may contribute to the maintenance of ZIP13 expression, although it is important to consider the possibility that the cell numbers may fall below the detection threshold because *Zip13*-KO showed the reduced number of quiescent MuSCs in FACS data. Previously, we reported that ZIP13 is involved in BMP/TGF-β signaling pathways[7], while it may be speculated that ZIP13-mediated activation of these pathways could amplify it expression, the precise molecular mechanisms should be addressed by further investigations. Because *Zip13-GFP*-KI mouse is a reporter mouse in which *Zip13* transcriptional expression (in other words, *Zip13* promoter activation) can be monitored by GFP in vivo and in vitro, investigation using the mouse will bring the exact molecular mechanism by which ZIP13 gene expression is regulated in not only MuSCs, but also the other cell types.

In this study, we demonstrated the following two issues: first, ZIP13 marks MuSCs and may play a role in regulating the balance of the quiescent and activated phases of MuSCs (Fig. 6); and second, the usefulness of *Zip13-GFP/Tomato*-KI mice in investigating the fate of ZIP13 expressing cells in vivo and in vitro. Due to

◀**Fig. 4**. The effect of ZIP13 on the regeneration of the skeletal muscle tissues in an acute muscle injury model. (**A**) Hematoxylin and eosin (H&E) staining of muscle tissue sections from $BaCl_2$-injected WT and *Zip13*-KO mice. White arrow indicates the nuclei around the muscle fibers. Black arrow indicates nuclei localization into the center of the muscle fibers. Higher magnification data surrounded in black squares in each H&E staining panel are presented below in each panel. The quantitative analysis of H&E staining was conducted. The perimeter (upper right) and cross sectional area (lower right) of the muscle fibers on Day 0 and Day 10 in both WT or *Zip13*-KO mice were shown as box-plot graphs. The Cohen's d values were also calculated and shown beneath each box-plot graphs. (**B**) Gene expression analysis of the skeletal muscle of either WT or *Zip13*-KO mice in a muscle injury model. The samples were collected on days 0, 5, and 10 after the $BaCl_2$ injection. Student's *t*-test was used to compare the two groups. The asterisk indicated a significant difference ($^*p < 0.05$, $^{**}p < 0.01$). Values are means ± S.E. of 3–5 mice. (**C**) GFP and Tomato fluorescent intensity of quiescent and activated phases of MuSCs, respectively were monitored using FACS and expressed as histogram. The MuSCs of *Zip13-GFP/Tomato*-KI mice on days 0, 20, and 30 after $BaCl_2$ injection were subjected to FACS analysis.

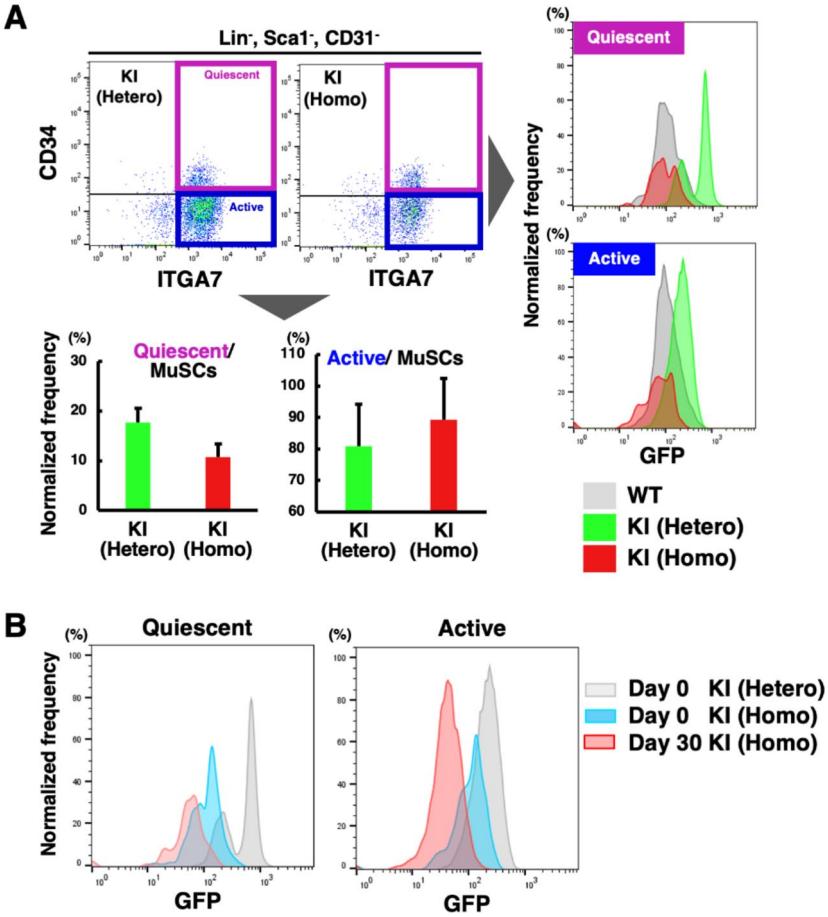

Fig. 5. ZIP13 expression regulation in the MuSCs of *Zip13-GFP*-KI homozygous mice. (**A**) The quiescent (blue square) and activated (purple square) phases of MuSCs either in heterozygous or homozygous *Zip13-GFP*-KI mice analyzed using FACS are shown as dot plots, and the cell numbers in each area normalized with $ITA7^+$ cell numbers are shown as bar graphs. The GFP fluorescence intensity of these two populations in WT (gray area), heterozygous (green area), and homozygous (red area) *Zip13-GFP*-KI mice are overlayed and shown as histograms. The GFP signal observed in the sample derived from the homozygous mice theoretically represents the promoter activity for *Zip13* mRNA expression. (**B**) The GFP fluorescence intensity of MuSCs of *Zip13-GFP*-KI homozygous mice subjected to the $BaCl_2$ acute injury model, was monitored using FACS. As compared to *Zip13-GFP*-KI heterozygous mice (gray area), *Zip13-GFP*-KI homozygous mice showed lowered GFP expression both on days 0 (blue area) and 30 (red area) after $BaCl_2$ injection. GFP expression of MuSCs were not recovered.

the lack of effective clinical treatments for skeletal muscle disorders especially such as frailty, sarcopenia, and cachexia[15,46], and such muscle dysfunctions are considered to be associated with zinc deficiency[15,46], elucidating the regulatory mechanisms of MuSCs and the role of zinc in their proper functions are highlighting further their importance as an integral component of the therapeutic cues[30]. Therefore, our findings suggest that ZIP13 is a

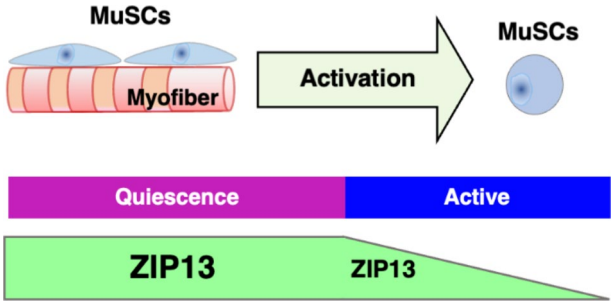

Fig. 6. A schematic diagram of ZIP13 expression in MuSCs during the transition of quiescent to activated phase. ZIP13 expression decreases during the transition to the activated phase of MuSCs, which may contribute to maintaining the quiescent phase of MuSCs.

novel regulatory molecule associated with MuSC homeostasis[15,46], and further research together with *Zip13-GFP/Tomato*-KI mouse may contribute to the development of innovative strategies for modulating MuSCs by fine-tuning ZIP13-mediated zinc homeostasis. Together with our previous reports[7,13,42], we believe we have been successful in creating a venue that highlights and explores the various facets and implications of ZIP13 in the muscle and MuSCs biology.

Methods

Animal experimentation and care

All procedures, including mouse handling, were approved by the Tokushima Bunri University Animal Care (Accession. No. 19 2) and Use Committee and by the Institutional Animal Care and Use Committee of RIKEN Kobe Branch. Also all methods were performed in accordance with relevant guidelines and regulations This study is reported in accordance with ARRIVE guidelines. The *Zip13-GFP*-KI mouse (Accession. No. CDB0085E: https://large.riken.jp/distribution/mutant-list.html) was generated by CRISPR/Cas9-mediated knock-in in zygotes as previously described[47]. The gRNA1 at the Zip13 locus (5'-TTT CTA GCG CCC GGC ATG CC-3') was designed by using CRISPRdirect (https://crispr.dbcls.jp)[48]. The donor vector which consists of microhomology arms and GFP-IRES-CreERT2[49] flanked by the gRNA2 site (5'-GCA TCG TAC GCG TAC GTG TT-3') was generated for the MMEJ (microhomology-mediated end joining)-based knock-in. For microinjection, a mixture of 2 crRNAs (CRISPR RNA) (50 ng/μl), tracrRNA (trans-activating crRNA) (200 ng/μl), donor vector (10 ng/μl), and Cas9 protein (100 ng/μl) were injected into C57BL/6 zygotes. The crRNA1 (5'-UUU CUA GCG CCC GGC AUG CCg uuu uag agc uau gcu guu uug-3'), the crRNA2 (5'-GCA UCG UAC GCG UAC GUG UUg uuu uag agc uau gcu guu uug-3') and tracrRNA (5'-AAA CAG CAU AGC AAG UUA AAA UAA GGC UAG UCC GUU AUC AAC UUG AAA AAG UGG CAC CGA GUC GGU GCU-3') were purchased from FASMAC. The actual knock-in mice were confirmed by PCR and sequencing. The PCR was performed by using primers; 5'FW: 5'-ACA TAG GCT GGA GCC AGC-3' and 5'REV: 5'-TTT ACG TCG CCG TCC AGC-3' (307 bp), and 3'FW: 5'-CGG ACC AAA GCC ACT TGG-3' and 3'REV: 5'-CTT TCC AGG AGC TCC AGG-3' (437 bp). The germline transmission of 2 mice were confirmed by genotyping of F1 mice. The mice (clone #39) were mainly used in this study.

The heterozygous *Zip13-GFP*-KI mice appeared phenotypically normal, and crosses between its heterozygotes produced homozygous mutant mice, according to Mendelian expectations. *Zip13*-KO mice were previously developed and maintained using a published genotyping method[7]. All mice were housed at a constant room temperature of 22℃, under 12 h light/dark cycle, and fed either a normal or a powder chow diet for WT, *Zip13-GFP*-KI, and *Zip13*-KO mice, respectively, with water *ad libitum*. Genotyping for *Zip13-GFP*-KI mouse was performed by PCR using LA Taq (Takara Bio, Inc. Shiga, Japan). The following primers were used for genotyping of *Zip13-GFP*-KI mice (Fig. 2A):

Cre-Forward; 5′-TTACGGCGCTAAGGATGACT-3′.
Cre-Reverse; 5′-TTGCCCCTGTTTCACTATCC-3′.
Z13-GFP-3 Forward; 5′-CGGACCAAAGCCACTTGG-3′.
Z13-GFP-3 Reverse; 5′- CTTTCCAGGAGCTCCAGG-3′.

Tamoxifen induction

Tamoxifen (Sigma-Aldrich, MO, USA) was dissolved in corn oil (Sigma-Aldrich) at a concentration of 20 mg/ml and then sonicated. The dissolved tamoxifen was protected from light with aluminum foil. Tamoxifen was administered at a dose of 75 mg/kg to a mouse by intraperitoneal injection every 24 h for 5 consecutive days (Supplemental Fig. 2).

Preparation of muscle satellite cells from mouse muscle tissue and FACS analysis

Muscle slurry was prepared from the hindlimb muscles, thigh, and spine muscles of 3- 6-weeks-old male C57BL/6, *Zip13-GFP*-KI, and *Zip13*-KO mice, as described by Gromova A. *et al.*[50]. Mononuclear cells were re-suspended in Dulbecco's modified Eagle's medium (DMEM) (FUJIFILM Wako Pure Chemical Corporation, Osaka, Japan) containing 2% Horse Serum (HS) (Sigma-Aldrich, MO, USA), 1% penicillin/streptomycin/Amphotericin (PSA) (Antibiotic-Antimycotic Mixed Stock Solution (100x), 1000units/ml Penicillin, 1000 μg/ml Streptomycin, 25 μg/ml Amphotericin B in 0.14% NaCl, 10nmol/L Citrate buffer; Stabilized) (nacalai tesque

inc, Kyoto, Japan). Cells were sorted using a BD FACSMelody Cell sorter (BD Biosciences, NJ, USA). Debris and dead cells were excluded using forward scatter, side scatter, and LIVE/DEAD Fixable Aqua Dead Cell Stain Kit (Thermo Fisher Scientific, CA, USA) gating. Those were incubated on ice for 30 min in the presence of APC-eFluor 780 anti-CD45 (clone: 30-F11, catalog number: 47-0451-82) (Invitrogen, MA, USA), Brilliant Violet 421 anti-CD11b (clone: M1/70, catalog number; 101236) (BioLegend, San Diego, USA), Brilliant Violet 421 anti-mouse CD31 (clone: 390, catalog number; 102424) (BioLegend, San Diego, USA), and Brilliant Violet 421 anti-mouse Ly-6 A/E (Sca-1) (clone: D7, catalog number; 108127) (BioLegend, San Diego, USA), then were washed with DMEM containing 2% HS. We isolated quiescent and activated MuSCs from mice based on the expression of PE anti-mouse ITGA7 (clone: 3C12, catalog number: K0046-5) (Medical & Biological Laboratories, Tokyo, Japan) and PE/Cyanine7 anti-mouse CD34 (clone: MEC14.7, catalog number: 119326) (BioLegend, San Diego, USA) for *Zip13*-KO and *Zip13-GFP*-KI mice. For the analysis of *Zip13-GFP/Tomato*-KI mouse, the live cells within the muscle slurry were stained with Brilliant Violet 421 anti-CD45 (clone: 30-F11, catalog number; 103134) (BioLegend, San Diego, USA), Brilliant Violet 421 anti-CD11b, Brilliant Violet 421 anti-mouse CD31, and Brilliant Violet 421 anti-mouse Sca-1, then stained with APC anti-mouse ITGA7 (clone: 334908, catalog number: FAB3518A) (R&D systems, MN, USA) and PE/Cyanine7 anti-mouse CD34. The gating strategies for FACS analysis were shown in Supplemental Fig. 1.

Muscle satellite cell isolation and immunostaining

Matrigel-coated dishes were prepared as described by Pasut A. *et al.*[51]. The muscle slurry was transferred to Matrigel (Sigma-Aldrich Co., LLC. MO, USA) precoated glass-bottom dishes (MATSUNAMI. Osaka, Japan) for 2 h in 37℃ CO_2 incubator, then washed with 0.1 M phosphate buffer (ph7.2) solution (PBS). Glass bottom dish was fixed with 4% paraformaldehyde/PBS within 8 min, rinsed with PBS 2X, 5 min each, then permeabilized with 0.3% Triton X-100/PBS for 10 min. The dish was then incubated with mouse IgG blocking solution from the M.O.M. Kit (Vector Lab) diluted in PBS/0.01% Triton X-100 following the dilution instructed in the manual. The dish was then incubated with PAX7 mouse monoclonal antibody (catalog number; sc-81648, Santa Cruz, CA, USA) and Alexa fluor 594 conjugated GFP polyclonal antibody (catalog number; A-21312, Invitrogen, MA, USA) diluted in the 2% FBS/ PBS overnight at light shielding 4℃. The next morning, the dish was washed 3X with 2% FBS/ PBS for 5 min each. A fluorescently conjugated secondary antibody (catalog number: ab96882, Abcam, Cambridge, UK) to species-specific IgG in blocking solution was applied at a 1/200 dilution for 1 h at room temperature. The dish was washed again with 2% FBS/ PBS. The dish was mounted in a Mounting Medium with DAPI (Vector Laboratories. Inc. CA. USA). All images were obtained under a fluorescence microscope BZ-X800 (Keyence Corporation, Osaka, Japan).

RNA extraction

Muscle tissue was suspended in 1 ml cold Sepasol-RNA I Super G regent (Nacalai Tasque, Kyoto, Japan). Zirconia/silica beads (5.5 g/cc, 3 mm in diameter; Bio Medical Science Inc. (BMS, Tokyo, Japan) were added to the cell suspensions. Bead beating for 30 s at 4000 rpm using a Homogenizer ShakeMan6 (BMS) was performed to completely break the cells and release nucleic acids from the samples. MuSCs were suspended in 1 ml TRIzol LS Reagent (Thermo Fisher Scientific, MA, USA). 200 µl of chloroform was added to each sample. The samples were then mixed by shaking for 30 s. The samples were then centrifuged at 15,000 × g for 15 min, and the supernatants were transferred to fresh 1.5 ml microtube. Transfer of Samples. (700 µl) were then mixed with the same volume of isopropanol. After incubation on ice for 10 min, the samples were centrifuged at 15,000 g for 20 min. Thereafter, the pellet was washed in 350 µl of 70% ethanol. The RNA extraction pellet obtained by centrifugation at 15,000 xg for 15 min, washed with ice-cold 70% ethanol, and dried. Finally, the dried RNA extraction samples were resuspended in 50 µl DNase, RNase-free UltraPure Distilled water (Invitrogen, NY, USA). RNA concentration (ng/µl) and quality (A260/A280; A260/A230) were determined using a DeNovix spectrophotometer (DS-11, SCRUM Inc., Tokyo, Japan).

Reverse transcription-polymerase chain reaction and primers

The 18S ribosomal (18S) RNA gene, a second housekeeping gene specific to mice, was amplified using specific primers.

18S-Foward (5′-AGTCCCTGCCCTTTGTACACA-3′) and Reverse (5′-GATCCGAGGGCCTCACTAAA C-3′).

The amplification of mice-specific *Zip13* (Forward; 5′-ACCGATGGACGGCAGCTAAG-3′, Reverse; 5′-AA CACATTCACCAGGGCGATATAGA-3′), *Pax7* (Forward; 5′-CCGTGTTTCCCATGGTTGTG-3,' Reverse; 5′-GAGCACTCGGCTAATCGAAC-3′), *Pax3* (Forward; 5′-TACCAGCCCACGTCTATTCCACAA-3,' Reverse; 5′-TTTGGTGTACAGTGCTCGGAGGAA-3′), *Myf5* (Forward; 5′-TGAGGGAACAGGTGGAGAAC-3,' Reverse; 5′-TGGAGAGAGGGAAGCTGTGT-3′), *Ki67* (Forward; 5′-AGGGCGGTGGGTCCAGTCGTAAC AGC-3,' Reverse; 5′-GCTATCTGCAGAAAGGCCCT-3′), *CD34* (Forward; 5′AAGGCTGGGTGAAGACCC TTA-3,' Reverse; 5′-TGAATGGCCGTTTCTGGAAGT-3′), *Atrogin-1* (Forward; 5′-GAGACCATTCTACAC TGGCAGCA-3, Reverse; 5′-GTCACTCAGCCTCTGCATGATGT-3′), *Foxo-1* (Forward; 5′-ACGAGTGGAT GGTGAAGAGC-3, Reverse; 5′-TGCTGTGAAGGGACAGATTG-3′), *MuRF* (Forward; 5′-ACCTGCTGGTG GAAAACATCATT-3,' Reverse; 5′-AGGAGCAAGTAGGCACCTCACAC-3′), *MyoD* (Forward; 5′-CCCCGG CGGCAGAATGGCTACG-3,' Reverse; 5′-GGTCTGGGTTCCCTGTTCTGTGT-3′), respectively. cDNA was synthesized using the PrimeScript RT Reagent Kit (Takara Bio, Shiga, Japan). Real-time quantitative RT-PCR analysis was performed in 20 µl reactions using Thunderbird Next SYBR qPCR Mix (TOYOBO, Osaka, Japan). The amplification protocol comprised 1 cycle at 95℃ for 1 min followed by 40 cycles at 95℃ for 5 s, and 60℃ for 20 s. Normalization was performed using 18S rRNA as an internal control. Each reaction was performed in

triplicate and six independent experiments were performed. The fold change in expression was then obtained by the $2^{-\Delta\Delta CT}$ method.

Statistical analysis

Data are presented as the mean ± standard error of the mean (SEM). Most experiments were repeated at least thrice. The results of the two experimental groups were compared using a two-tailed unpaired Student's *t*-test. Statistically significant values of $p < 0.05$ and $p < 0.01$ by two-tailed Student's *t*-test are indicated by asterisks (*) and (**) respectively.

Muscle injury procedure

All muscle injury procedures were performed under inhaled isoflurane anesthesia with a mixture of oxygen and room air. To induce muscle regeneration, three doses of 10 µl of 1.2% $BaCl_2$ (barium chloride) solution (FUJIFILM Wako Pure Chemical Corporation, Osaka, Japan) dissolved in phosphate-buffered saline (PBS) was administered in each leg TA/GAS muscles of mice with a 30-gauge needle. At various time points after the injury, the mice were weighed and sacrificed by cervical dislocation.

Histological analysis

After euthanasia and sacrifice, the TA muscles were quickly harvested 5 and 10 days after $BaCl_2$ injection. The tissue samples were immediately frozen in liquid nitrogen-cooled isopentane.

Serial longitudinal sections of muscle tissues were cut at 8 µm using a Leica CM1520 cryostat (Leica Biosystems, IL, USA). The object temperature was set to -18℃, and the ambient cryostat temperature was set to -20℃. A flat cold tissue on the cork that had been removed from -80℃ was placed in the cryostat immediately before sectioning. Samples were removed from isopentane and promptly affixed to the object disc of the cryostat using Tissue-Tek Optional Cutting Temperature (OCT) media (Sakura-Finetek, CA, USA). The fixed tissues were allowed to equilibrate in a cryostat environment for 10 min before sectioning. Muscle cryostat sections were stained with hematoxylin and eosin (H&E). Serial cross-sections were blocked with 5% goat serum in PBS then sections were observed under a fluorescence microscope BZ-X800 (Keyence Corporation, Osaka, Japan).

Data availability

The *Zip13-GFP*-KI mouse is available in the database of RIKEN BDR (Accession. No. CDB0085E: https://large.riken.jp/distribution/mutant-list.html). All data generated or analyzed during this study are included in this published article. The data used and/or analyzed during the current study are available from corresponding authors upon reasonable request.

Received: 5 September 2024; Accepted: 27 February 2025
Published online: 17 March 2025

References

1. Hara, T. et al. Physiological roles of zinc transporters: molecular and genetic importance in zinc homeostasis. *J. Physiol. Sci.* **67**, 283–301 (2017).
2. Abeywickrama, H. M., Uchiyama, M., Sumiyoshi, T., Okuda, A. & Koyama, Y. The role of zinc on nutritional status, sarcopenia, and frailty in older adults: a scoping review. *Nutr. Rev.* **82**, 988–1011 (2024).
3. Prasad, A. S., Halsted, J. A. & Nadimi, M. Syndrome of iron deficiency anemia, hepatosplenomegaly, hypogonadism, dwarfism and geophagia. *Am. J. Med.* **31**, 532–546 (1961).
4. Prasad, A. S. Discovery of human zinc deficiency: its impact on human health and disease. *Adv. Nutr.* **4**, 176–190 (2013).
5. Fukada, T. Late Prof Dr. Ananda Prasad 'the legend and the father of zinc biology'. *J. Trace Elem. Med. Biol.* **80**, 127276 (2023).
6. Hara, T., Yoshigai, E., Ohashi, T. & Fukada, T. Zinc transporters as potential therapeutic targets: an updated review. *J. Pharmacol. Sci.* **148**, 221–228 (2022).
7. Fukada, T. et al. The zinc transporter SLC39A13/ZIP13 is required for connective tissue development; its involvement in BMP/TGF-beta signaling pathways. *PLoS One* **3**, e3642 (2008).
8. Giunta, C. et al. Spondylocheiro dysplastic form of the Ehlers-Danlos syndrome–an autosomal-recessive entity caused by mutations in the zinc transporter gene SLC39A13. *Am. J. Hum. Genet.* **82**, 1290–1305 (2008).
9. Bin, B. H. et al. Molecular pathogenesis of spondylocheirodysplastic Ehlers-Danlos syndrome caused by mutant ZIP13 proteins. *EMBO Mol. Med.* **6**, 1028–1042 (2014).
10. Bin, B. H. et al. Biochemical characterization of human ZIP13 protein: a homo-dimerized zinc transporter involved in the Spondylocheiro dysplastic Ehlers-Danlos syndrome. *J. Biol. Chem.* **286**, 40255–40265 (2011).
11. Kumps, C. et al. The connective tissue disorder associated with recessive variants in the SLC39A13 zinc transporter gene (Spondylo-Dysplastic Ehlers–Danlos syndrome type 3): insights from four novel patients and Follow-Up on two original cases. *Genes* **11**, 420 (2020).
12. Agrawal, P., Kaur, H., Kondekar, A. & Rathi, S. A case of Ehlers-Danlos syndrome presenting as short stature: a novel mutation in SLC39A13 causing spondylodysplastic Ehlers-Danlos syndrome. *Oxf. Med. Case Rep.* **2023**, omac107 (2023).
13. Shoji, M. et al. Possible involvement of zinc transporter ZIP13 in myogenic differentiation. *Sci. Rep.* **14**, 8052 (2024).
14. Chargé, S. B. P. & Rudnicki, M. A. Cellular and molecular regulation of muscle regeneration. *Physiol. Rev.* **84**, 209–238 (2004).
15. Chakkalakal, J. V., Jones, K. M., Basson, M. A. & Brack, A. S. The aged niche disrupts muscle stem cell quiescence. *Nature* **490**, 355–360 (2012).
16. Lepper, C., Partridge, T. A. & Fan, C. M. An absolute requirement for Pax7-positive satellite cells in acute injury-induced skeletal muscle regeneration. *Development* **138**, 3639–3646 (2011).
17. Kassar-Duchossoy, L. et al. Pax3/Pax7 mark a novel population of primitive myogenic cells during development. *Genes Dev.* **19**, 1426–1431 (2005).
18. Brack, A. S. Pax7 is back. *Skelet. Muscle.* **4**, 24 (2014).
19. von Maltzahn, J., Jones, A. E., Parks, R. J. & Rudnicki, M. A. Pax7 is critical for the normal function of satellite cells in adult skeletal muscle. *Proc. Natl. Acad. Sci. U. S. A.* **110**, 16474–16479 (2013).
20. Seale, P. et al. Pax7 is required for the specification of myogenic satellite cells. *Cell* **102**, 777–786 (2000).

21. Sambasivan, R. et al. Pax7-expressing satellite cells are indispensable for adult skeletal muscle regeneration. *Development* **138**, 3647–3656 (2011).
22. Cooper, R. N. et al. In vivo satellite cell activation via Myf5 and myod in regenerating mouse skeletal muscle. *J. Cell. Sci.* **112** (Pt 17), 2895–2901 (1999).
23. Hasty, P. et al. Muscle deficiency and neonatal death in mice with a targeted mutation in the Myogenin gene. *Nature* **364**, 501–506 (1993).
24. Nabeshima, Y. et al. Myogenin gene disruption results in perinatal lethality because of severe muscle defect. *Nature* **364**, 532–535 (1993).
25. Cornelison, D. D. & Wold, B. J. Single-cell analysis of regulatory gene expression in quiescent and activated mouse skeletal muscle satellite cells. *Dev. Biol.* **191**, 270–283 (1997).
26. Günther, S. et al. Myf5-positive satellite cells contribute to Pax7-dependent long-term maintenance of adult muscle stem cells. *Cell. Stem Cell.* **13**, 590–601 (2013).
27. Ott, M. O., Bober, E., Lyons, G., Arnold, H. & Buckingham, M. Early expression of the myogenic regulatory gene, myf-5, in precursor cells of skeletal muscle in the mouse embryo. *Development* **111**, 1097–1107 (1991).
28. Sousa-Victor, P., García-Prat, L. & Muñoz-Cánoves, P. Control of satellite cell function in muscle regeneration and its disruption in ageing. *Nat. Rev. Mol. Cell. Biol.* **23**, 204–226 (2022).
29. Bentzinger, C. F., Wang, Y. X. & Rudnicki, M. A. Building muscle: molecular regulation of myogenesis. *Cold Spring Harb Perspect. Biol.* **4**, a008342 (2012).
30. Wang, Y. X. & Rudnicki, M. A. Satellite cells, the engines of muscle repair. *Nat. Rev. Mol. Cell. Biol.* **13**, 127–133 (2012).
31. Rudnicki, M. A., Le Grand, F., McKinnell, I. & Kuang, S. The molecular regulation of muscle stem cell function. *Cold Spring Harb. Symp. Quant. Biol.* **73**, 323–331 (2008).
32. Kuang, S., Gillespie, M. A. & Rudnicki, M. A. Niche regulation of muscle satellite cell self-renewal and differentiation. *Cell. Stem Cell.* **2**, 22–31 (2008).
33. Hawke, T. J. & Garry, D. J. Myogenic satellite cells: physiology to molecular biology. *J. Appl. Physiol. 1985* **91**, 534–551 (2001).
34. Li, S. et al. Dual fluorescent reporter pig for Cre recombination: transgene placement at the ROSA26 locus. *PLoS One* **9**, e102455 (2014).
35. Jung, H. W., Choi, J. H., Jo, T., Shin, H. & Suh, J. M. Systemic and local phenotypes of barium chloride induced skeletal muscle injury in mice. *Ann. Geriatr. Med. Res.* **23**, 83–89 (2019).
36. Nishino, I. ABC in muscle pathology. *Rinsho Shinkeigaku*. **51**, 669–676 (2011).
37. Gumucio, J. P. & Mendias, C. L. Atrogin-1, MuRF-1, and sarcopenia. *Endocrine* **43**, 12–21 (2013).
38. Ohashi, W., Hara, T., Takagishi, T., Hase, K. & Fukada, T. Maintenance of intestinal epithelial homeostasis by zinc transporters. *Dig. Dis. Sci.* **64**, 2404–2415 (2019).
39. Schmidt, M., Schüler, S. C., Hüttner, S. S., von Eyss, B. & von Maltzahn, J. Adult stem cells at work: regenerating skeletal muscle. *Cell. Mol. Life Sci.* **76**, 2559–2570 (2019).
40. Fukada, S. I. et al. Isolation, characterization, and molecular regulation of muscle stem cells. *Front. Physiol.* **4**, 317 (2013).
41. Dumont, N. A., Wang, Y. X. & Rudnicki, M. A. Intrinsic and extrinsic mechanisms regulating satellite cell function. *Development* **142**, 1572–1581 (2015).
42. Hara, T. et al. Role of Scl39a13/ZIP13 in cardiovascular homeostasis. *PLoS One* **17**, e0276452 (2022).
43. Alfaro, L. A. S. et al. CD34 promotes satellite cell motility and entry into proliferation to facilitate efficient skeletal muscle regeneration. *Stem Cells* **29**, 2030–2041 (2011).
44. Rocheteau, P., Gayraud-Morel, B., Siegl-Cachedenier, I., Blasco, M. A. & Tajbakhsh, S. A subpopulation of adult skeletal muscle stem cells retains all template DNA strands after cell division. *Cell* **148**, 112–125 (2012).
45. Rodgers, J. T. et al. mTORC1 controls the adaptive transition of quiescent stem cells from G0 to GAlert. *Nature* **510**, 393–396 (2014).
46. Reddy, S. S., Addi, U. R., Pullakhandam, R. & Reddy, G. B. Dietary zinc deficiency disrupts skeletal muscle proteostasis and mitochondrial biology in rats. *Nutrition* **98**, 111625 (2022).
47. Abe, T., Inoue, K. I., Furuta, Y. & Kiyonari, H. Pronuclear microinjection during S-Phase increases the efficiency of CRISPR-Cas9-Assisted knockin of large DNA donors in mouse zygotes. *Cell. Rep.* **31**, 107653 (2020).
48. Naito, Y., Hino, K., Bono, H. & Ui-Tei, K. CRISPRdirect: software for designing CRISPR/Cas guide RNA with reduced off-target sites. *Bioinformatics* **31**, 1120–1123 (2015).
49. Snippert, H. J. et al. Lgr6 marks stem cells in the hair follicle that generate all cell lineages of the skin. *Science* **327**, 1385–1389 (2010).
50. Gromova, A., Tierney, M. T. & Sacco, A. FACS-based satellite cell isolation from mouse Hind limb muscles. *Bio-Protoc* **5**, e1558 (2015).
51. Pasut, A., Jones, A. E. & Rudnicki, M. A. Isolation and culture of individual myofibers and their satellite cells from adult skeletal muscle. *J. Vis. Exp.* (73), e50074 (2013).

Acknowledgements

The plasmid coding EGFP-IRES-CreERT2 cassette was kindly gifted from Drs. Hans Clevers and Marc van de Wetering, Hubrecht Institute–KNAW (Royal Netherlands Academy of Arts and Sciences) and University Medical Center Utrecht, Netherlands. This study was supported by grants from the Japan Society for the Promotion of Science KAKENHI (21J40212, 22K11871, 22KJ3069), Urakami Foods and Food Culture Promotion Foundation (to EY), as well as the Japan Society for the Promotion of Science KAKENHI (20H03409), research grant of the Princess Takamatsu Cancer Research Fund, SECOM Science and Technology Foundation, Terumo Life Science Foundation, The Uehara Memorial Foundation, Astellas Foundation for Research on Metabolic Disorders, the joint research program of the Institute for Molecular and Cellular Regulation, Gunma University, The Science Research Promotion Fund (to TF), and KAKENHI (18K06711, 23K05687), Koyanagi-Foundation, the Naitou Foundation, the Mochida Memorial Foundation for Medical and Pharmaceutical Research, and KOSE Cosmetology Research Foundation (to TH).

Author contributions

E.Y. and T.H. contributed equally to this study. E.Y. designed the study, performed experiments with MuSCs and mouse model, analyzed the data, and wrote the manuscript. T.A. and K.I. developed the KI mice. T.H. T.O., H.T., M.H. and A. N. performed the experiments using MuSCs, FACS, and the data analysis. E.Y., T.H., and T.F. designed the study, wrote and supervised the manuscript.

Declarations

Competing interests
The authors declare no competing interests.

Additional information
Supplementary Information The online version contains supplementary material available at https://doi.org/10.1038/s41598-025-92501-y.

Correspondence and requests for materials should be addressed to E.Y. or T.F.

Reprints and permissions information is available at www.nature.com/reprints.

Publisher's note Springer Nature remains neutral with regard to jurisdictional claims in published maps and institutional affiliations.